FEBS Letters 581 (2007) 5677–5684

Role of the arginine finger in Ras·RasGAP revealed by QM/MM calculations

Henrik te Heesen, Klaus Gerwert, Jürgen Schlitter*

Department of Biophysics, ND 04 North, University of Bochum, D-44780 Bochum, Germany

Received 12 July 2007; revised 12 October 2007; accepted 7 November 2007

Available online 20 November 2007

Edited by Robert B. Russell

Abstract In the Ras·RasGAP complex, hydrolysis of guanosine triphosphate is strongly accelerated GAP as compared to Ras alone. This is largely attributed to the arginine finger $R789^{GAP}$ pointing to AlF_x in the transition state analogue. We performed QM/MM simulations where triphosphate was treated using the quantum mechanical method of density functional theory, while the protein complex and water environment were described classically using MD. Compared to Ras, the crucial electron shift, bond stretching and distortion towards an eclipsed γ-to-β orientation are much more pronounced. The arginine finger is shown to act by displacing water out of the binding niche. The resulting enhanced electrostatic field catalyses the cleavage step.

Keywords: Ras; Ras·RasGAP; GTP hydrolysis; Arginine finger; QM/MM; Electrostatic catalysis

1. Introduction

The GTPase Ras p21 is a crucial switch in cellular signal transduction [1]. In ON state the substrate guanosine triphosphate (GTP) is bound to the enzyme Ras; in OFF state guanosine diphosphate (GDP) is bound. Ras is deactivated by GTP hydrolysis to GDP and P_i. The bond between P_γ and $O_{3\beta}$ of GTP is cleaved by nucleophilic attack of a water molecule which binds at the γ-phosphate [2]. Activated Ras interacts with effector proteins, transmitting, e.g. the cell growth signal to the nucleus [3]. The GTPase-activating protein (GAP) docking to Ras accelerates GTP hydrolysis by a factor of 10^5 and thus regulates the process [4]. Inactive Ras is reactivated by a guanine exchange factor (GEF) catalysing the exchange of GDP by GTP.

The hydrolysis reactions of Ras and Ras·RasGAP have been investigated by time-resolved Fourier transform infrared (tr-FTIR) difference spectroscopy [5–10]. FTIR spectra of the substrate GTP show remarkable changes when the substrate binds to Ras in comparison to experiments in water. The addition of RasGAP provides only minor changes in the GTP spectrum. The results were interpreted as caused by electron charge shift towards the β-phosphate due to enzyme binding, i.e. a charge distribution close to the product state [8,11]. This seems to be a common feature of proteins of the Ras superfamily, as for example tr-FTIR measurements of the Rap·RapGAP complex demonstrate a similar behaviour [12].

Several groups have investigated GTP hydrolysis by QM and combined QM/MM calculations. Warshel and co-workers [13] found by applying the empirical valence bond (EVB) method to different phosphate monoester di-anions in solutions and proteins that a slightly more associative pathway is preferred in the protein-environment [14]. Their energy profiles are comparable to experimental data [15]. Grigorenko et al. have analysed the energy barriers of dissociative GTP hydrolysis in water [16], bound to Ras [17] and to Ras·RasGAP [18,19]. They observed a stretching of the P_γ-$O_{3\beta}$ bond in Ras·RasGAP compared to Ras and impairment of catalysis by the mutation R789L. The change of their charge distribution of the triphosphate group of GTP in Ras and Ras·RasGAP is comparable to the charge distribution determined by Klähn [20]. Futatsugi et al. showed that $K16^{Ras}$ plays a key role for the molecular switching mechanism in Ras [21,22] and Giα1 [23].

We investigated the influence of Ras and Ras·RasGAP on the substrate GTP in the reactant state by QM/MM calculations. In a previous study QM/MM simulations were performed of Ras with a sodium ion close to γ-phosphate [20]. In our analysis triphosphate is treated using a quantum mechanical method, protein and bulk water are described by a classical molecular mechanics (MM) force field. We calculate vibrational spectra of TP in harmonic approximation and compare them with experimental data [7,8] in order to scrutinise the structure of the substrate under spectral control. Provided that the calculated IR spectra reproduce experimental FTIR data within computational accuracy, we determine charge distribution and structural details of our sampled structures. For the comprehension of the electron shift on TP, the electric field exerted by the protein and solvent is analysed. We can specify the components, especially due to $K16^{Ras}$, Mg^{2+}, $R789^{GAP}$ and water molecules which are directly involved in varying the charge distribution. This novel approach is suitable for explaining the catalytic action of GAP on GTP hydrolysis.

2. Methods

2.1. Applied simulation method

In addition to TP, the QM part compromises the next CH_2 and a link atom H which together form a methyl group [20]. For our QM/MM calculations we used EGO-MMII-1-2 [24] for MD and CPMD 3.9.2 [25] for QM. A fast multipole method combined with a reaction field is used for long-range electrostatics [26] in EGO. The electrostatics within

*Corresponding author. Fax: +49 234 3214626.
E-mail address: juergen.schlitter@rub.de (J. Schlitter).

0014-5793/$32.00
doi:10.1016/j.febslet.2007.11.026

the simulation cell are treated by a structure-adapted multipole method for electrostatic interactions [27,28] and a hybrid method for exchanging Coulomb interaction of the classical and quantum mechanical parts [29]. The charges of QM atoms are calculated using ESP [30]. Covalent bonds between QM and MM are described by a scaled position link atom method (SPLAM) [29].

For the DFT Hamiltonian, the functionals of Becke [31] and Perdew [32] (BP86) and the pseudopotentials from Hartwigsen (HGH) [33] were used with a cut-off of 80 Ry. The classical part of the simulation system containing the guanosine, the protein complex, TIP3P water molecules, and the counter ions were described by the CHARMM22 force field [34]. The MM parameters for TP were taken from Klähn [20]. A detailed description of the applied simulation method can be found in [20,35,36].

2.2. QM/MM simulations

Two separate simulations were performed. First, we analysed the influence of the Ras p21 protein on GTP. Secondly, we studied the Ras·RasGAP complex. The initial atom positions have been taken from the protein data bank (PDB-ID for Ras: 1QRA [37], PDB-ID for Ras·RasGAP: 1WQ1 [38]). Aluminium fluoride of the Ras·RasGAP transition state analogue structure was replaced by a phosphate. The hydrogen bond network was determined using the HB2 algorithm implemented in the WHAT IF program [39]. The protein was inserted in a rhombic dodecahedric simulation cell filled with 12578 water molecules in the case of Ras and 37315 water molecules in the case of Ras·RasGAP. 39 Na^+ and 32 Cl^- ions were added to the Ras and 111 Na^+ and 97 Cl^- ions to the Ras·RasGAP system in order to obtain a natural salt concentration of 155 mmol/l and an electric neutral simulation cell (see Fig. 1 for the Ras·RasGAP simulation system and Fig. 2 for a detailed view of the substrate and its environment). The systems were energy minimised, heated and equilibrated for 1000 ps. Subsequently, a free MD simulation was executed for 500 ps with a time step of 1 fs at a temperature of 300 K. Six Ras snapshots, respectively seven Ras·RasGAP snapshots, were taken from the MD runs as starting points for QM/MM calculations in the ground state.

For each snapshot, QM/MM trajectories with a step size of 0.25 fs were computed for 150 fs at a temperature of 300 K. Structural details and charge distribution were derived by averaging the last 500 integration steps of these trajectories. The first 100 steps are neglected in order to let the system relax after changing the force field from MM to QM/MM. The last structure of each snapshot is taken for a severe QM/MM energy minimisation. The energetic minimum is the basic structure for calculating the Hesse matrix. The eigenvalues and eigenvectors for the IR spectrum are derived using the instantaneous normal mode analysis (INMA). The ESP charges from the trajectories and the single spectra are averaged over all snapshots.

3. Results

The simulations were evaluated to obtain spectral and structural data suitable for verifying the quality of computations and providing insight into the catalytic action of Ras.

We determined the IR spectra of GTP bound to Ras and to Ras·RasGAP as shown in Fig. 3 and compared the results with experimental data [5–9]. The modes were assigned to the measured bands by inspecting the mass-weighted normal modes. Symmetric and asymmetric bond stretching modes involving non-bridging oxygens are denoted by $\nu_{a/s}(PO_{2/3})_{\alpha/\beta/\gamma}$, symmetric and asymmetric stretching modes with bridging oxygens are denoted by $\nu_{a/s}(OP_\beta O)$. The last index designates the phosphate group involved in PO stretch vibrations. We can assign

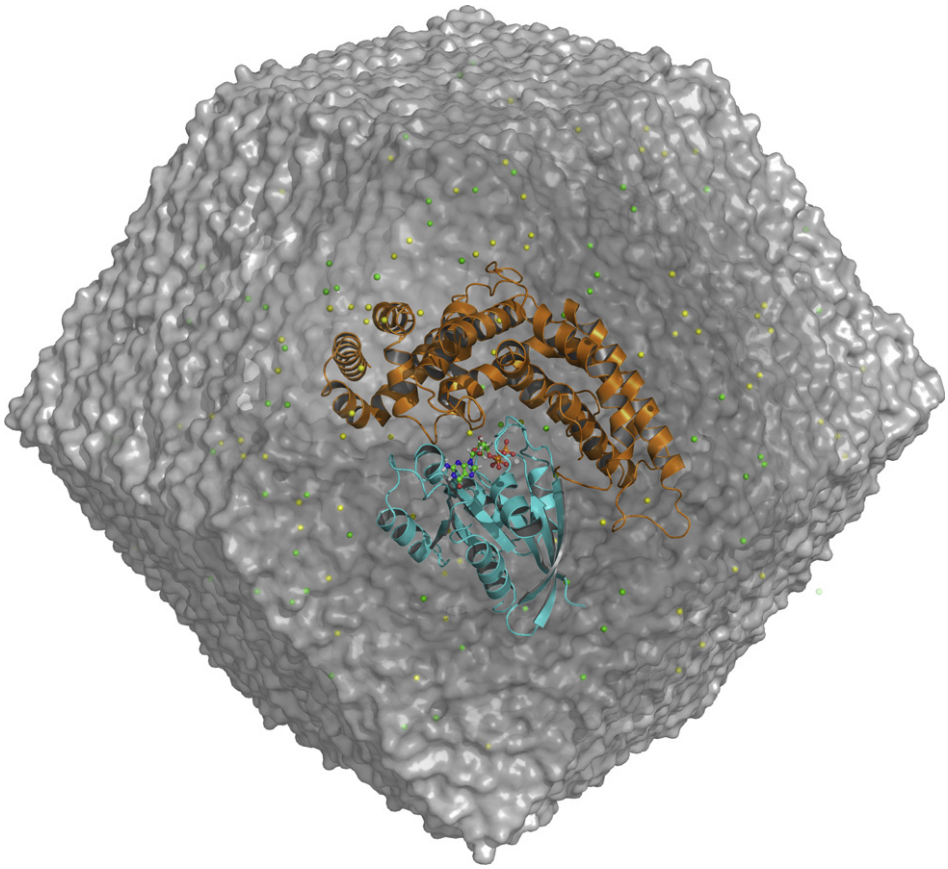

Fig. 1. The rhombic dodecahedric simulation cell of the equilibrated Ras·RasGAP complex. Ras is shown in cyan, GAP in orange, sodium ions in yellow, chloride in green, the substrate GTP in ball and sticks. The whole simulation system contains 119995 atoms and has a radius of 60.0 Å.

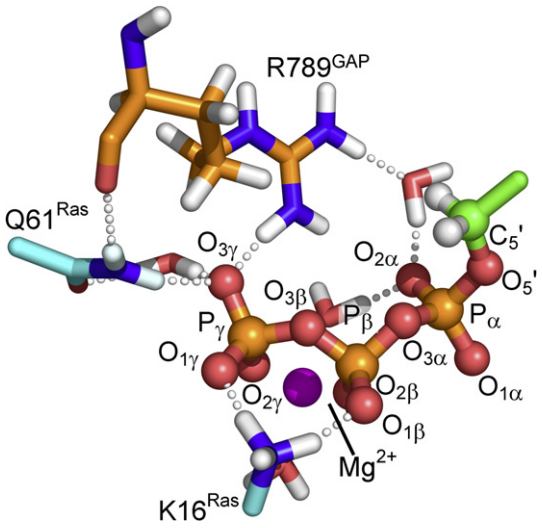

Fig. 2. Snapshot of the environment of the TP derived from QM/MM simulation. Atoms of GTP that are treated quantum mechanically are shown in ball and sticks, Ras is cyan, GAP is orange. The amino acids $K16^{Ras}$, $Q61^{Ras}$ and $R789^{GAP}$ and all water molecules in the binding niche are shown as sticks, the magnesium ion is shown in magenta. In the nucleophilic attack the water molecule approaches the γ-phosphate from the left by directing its oxygen.

more low-lying modes of bond stretching, angle bending, and torsion twisting, but these modes have not yet been identified by FTIR measurements. The relative deviation of our band positions of 3.2% is within the computational accuracy of DFT.

Structural deviations can be identified clearly in calculated spectra as the bands are up or down shifted. For instance, if the water molecule between the amino group of $R789^{GAP}$ and P_α is omitted and a direct hydrogen bond between $R789^{GAP}$ and $O_{2\alpha}$ is formed, the $\nu_a(PO_2)_\alpha$ band is blue shifted from 1256 cm^{-1} to 1341 cm^{-1} (see Fig. 2).

To quantify if our QM/MM trajectories are sufficiently equilibrated, we compare the slowest bands, the $\nu_{a/s}(OP_\beta O)$ bands, with experimental ones. If the quantum box is not in equilibrium, the angle stretching vibrations will be blue shifted as the distances inside the triphosphate backbone are too short. We clearly see that our angle stretching vibrations are very close to the experimental ones and thus our quantum mechanically treated subsystem is equilibrated.

Using FTIR measurements, two $\nu_a(PO_2)_\beta$ vibrations at 1217 cm^{-1} and 1140 cm^{-1} were identified in the Ras·RasGAP complex. As mentioned above, the lower band at 1140 cm^{-1} is being discussed [10]. Nevertheless, we could reproduce this second asymmetric β-band by deprotonating $K16^{Ras}$ and protonating $O_{1\beta}$ of β-phosphate. In this case, the calculated asymmetric β-band at 1188 cm^{-1} disappears and a new band appears at 1124 cm^{-1}. The red shift of 64 cm^{-1} is significantly larger than the computational accuracy and comparable to the experimental red-shift of 77 cm^{-1}. Likewise, the protonation of β-phosphate leads to a red-shift of the symmetric β-band from 1046 cm^{-1} to 900 cm^{-1}. This shift has not been observed by FTIR, probably because symmetric vibrations have a weak intensity. The idea of a shared proton between $K16^{Ras}$ and $O_{1\beta}$ has been discussed by Futatsugi [22] and Cavalli [40]. We will present our detailed analysis of indications of a shared proton due to a low energy hydrogen bond elsewhere. Its possible occurrence does not influence our conclusions in this publication.

In Table 1, we compare the structural details of TP in Ras and Ras·RasGAP. The values are double averages over the

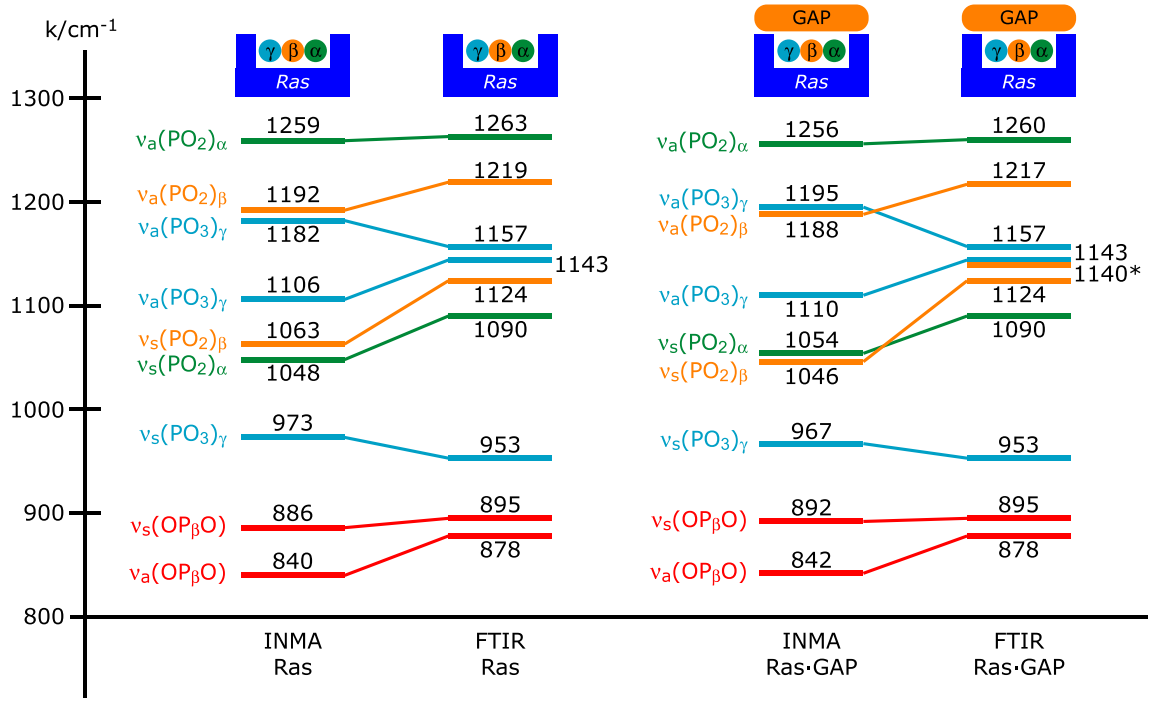

Fig. 3. IR absorption frequencies calculated for Ras (left columns) and Ras·RasGAP (right columns). The values calculated with the INMA protocol are shown on the left-hand side of the columns, the measured frequencies are shown on the right-hand side. FTIR data for Ras is taken from Cepus [5] and Allin [7], FTIR data for Ras·RasGAP is taken from Allin [8] and Kötting [9]. The assignment of types of vibrations are given on the left-hand side of the columns. The additional $\nu_a(PO_2)_\beta$, marked by *, is discussed in the text.

Table 1
Calculated structural details of the TP bound to Ras and Ras·RasGAP

Distance (Å)	P_γ–$O_{1\gamma}$	P_γ–$O_{2\gamma}$	P_γ–$O_{3\gamma}$	P_γ–$O_{3\beta}$
Ras	1.52 ± 0.03	1.55 ± 0.04	1.55 ± 0.03	1.76 ± 0.06
Ras·RasGAP	1.51 ± 0.02	1.54 ± 0.03	1.50 ± 0.02	1.83 ± 0.09
Distance (Å)	P_β–$O_{1\beta}$	P_β–$O_{2\beta}$	P_β–$O_{3\beta}$	P_β–$O_{3\alpha}$
Ras	1.51 ± 0.04	1.53 ± 0.03	1.62 ± 0.04	1.62 ± 0.04
Ras·RasGAP	1.51 ± 0.04	1.53 ± 0.03	1.62 ± 0.04	1.64 ± 0.05
Distance (Å)	P_α–$O_{1\alpha}$	Pα–$O_{2\alpha}$	P_α–$O_{3\alpha}$	Pα–O'_5
Ras	1.49 ± 0.03	1.50 ± 0.03	1.71 ± 0.05	1.68 ± 0.05
Ras·RasGAP	1.49 ± 0.02	1.50 ± 0.02	1.68 ± 0.05	1.70 ± 0.05
Distance (Å)	O'_5–C'_5	$O_{2\gamma}$–$O_{2\beta}$	P_γ–P_β	$O_{2\gamma}$–Mg^{2+}
Ras	1.46 ± 0.03	3.51 ± 0.20	3.19 ± 0.09	1.92 ± 0.04
Ras·RasGAP	1.46 ± 0.03	3.51 ± 0.19	3.26 ± 0.10	1.91 ± 0.04
Distance (Å)	$O_{2\beta}$–Mg^{2+}	$O_{1\gamma}$–$H^{K16}_{3\zeta}$	$O_{1\beta}$–$H^{K16}_{3\zeta}$	$O_{3\gamma}$–HH^{R789}_{12}
Ras	1.97 ± 0.09	1.63 ± 0.08	1.82 ± 0.11	—
Ras·RasGAP	1.97 ± 0.08	1.64 ± 0.09	1.72 ± 0.10	1.74 ± 0.10
Angle (°)	∠P_γ–$O_{3\beta}$–Pβ	∠$O_{3\beta}$–P_β–$O_{3\alpha}$	∠P_β–$O_{3\alpha}$–P_α	∠$O_{3\alpha}$–P_α– O'_5
Ras	142.7 ± 9.4	105.6 ± 5.1	125.5 ± 4.2	96.7 ± 3.3
Ras·RasGAP	143.3 ± 8.2	105.5 ± 5.8	125.3 ± 3.8	96.1 ± 2.9
Angle (°)	∠P_α–O'_5–C'_5	∠$O_{1\gamma}$–Pγ–$O_{3\beta}$	∠$O_{2\gamma}$–P_γ– $O_{3\beta}$	∠$O_{3\gamma}$–P_γ–$O_{3\beta}$
Ras	119.8 ± 4.3	107.7 ± 4.2	103.9 ± 6.4	100.9 ± 4.2
Ras·RasGAP	117.6 ± 3.9	106.7 ± 4.2	101.9 ± 4.3	100.9 ± 3.8
Dihedral (°)	$O_{2\gamma}$–P_γ–$O_{3\beta}$–P_β	$O_{2\gamma}$–P_γ–P_β–$O_{2\beta}$		
Ras	−60.5 ± 17.2	−5.5 ± 5.1		
Ras·RasGAP	−58.6 ± 11.6	0.6 ± 3.9		

The atom names are denoted in Fig. 2. The values are double averages over the QM/MM trajectories. The distances are given in Å, the angles and dihedral angles are given in °. The addition of GAP shows remarkable changes for a few properties. Most values are identical, but the P_γ–$O_{3\beta}$ bond is weakened and therefore the distance between P_γ and P_β increases, $K16^{Ras}$ is moved towards β-phosphate and the dihedral angle $O_{2\gamma}$–P_γ–P_β–$O_{2\beta}$ appears perfectly eclipsed.

QM/MM trajectories. Adding GAP to the enzyme-substrate complex, Ras·GTP induces few remarkable changes at localised properties. Most distances, bond angles and dihedral angles are unchanged. Especially the distances of the non-bridging oxygens to phosphorus and the calculated stretch vibrations $\nu_{a/s}(PO_{2/3})$ are practically the same. As the agreement of these vibrational bands is also observed in FTIR experiments, we must conclude that the PO distances do not change much when going from Ras to Ras·RasGAP.

However, GAP weakens the crucial bond between P_γ and $O_{3\beta}$ which is hence elongated from 1.76 Å in Ras to 1.83 Å in Ras·RasGAP. Also the distance between P_γ and P_β increases from 3.19 Å in Ras to 3.26 Å in Ras·RasGAP. The distance between $K16^{Ras}$ and β-phosphate is shortened from 1.82 Å in Ras to 1.72 Å in Ras·RasGAP. The dihedral angle $O_{2\gamma}$–P_γ–P_β– $O_{2\beta}$ changes from −5.5° in Ras to an almost perfectly eclipsed conformation of 0.6° in Ras·RasGAP. Our results reproduce the trend of the enzyme action on structural details of Klähn et al. [20] and Grigorenko et al. [17].

Next, we take a detailed look at the charge distribution of TP (see Table 2). We used ESP partial charges for all atoms of TP. The two oxygens $O_{2\gamma}$ and $O_{2\beta}$ directing towards the magnesium ion have slightly more negatively charged than the other oxygens of γ- and β-phosphate interacting with $K16^{Ras}$ and $R789^{GAP}$. Negative charge accumulates at $O_{3\beta}$. The total charge of β-phosphate has the same value in Ras and Ras·RasGAP. The addition of GAP leads to a more positively charged γ- and a more negative charges α-phosphate. The methyl group shows no change when GAP is added to the Ras·GTP complex. This was also observed by Grigorenko et al. [17] although their charge distribution seems to be too polar for describing a correct interaction with the surrounding atoms treated classically. Our partial charges correspond to those of Klähn without taking the putative sodium ion into consideration [20].

Table 2
ESP charges of the TP bound to Ras and Ras·RasGAP obtained from double averaging the QM/MM trajectories

	P_γ	$O_{1\gamma}$	$O_{2\gamma}$	$O_{3\gamma}$		$\sum_\gamma$
Ras	+1.55	−0.97	−1.11	−0.91		−1.44
Ras·RasGAP	+1.52	−0.92	−1.08	−0.87		−1.35
	P_β	$O_{1\beta}$	$O_{2\beta}$	$O_{3\beta}$	$O_{3\alpha}$	$\sum_\beta$
Ras	+1.13	−0.84	−1.01	−0.78	−0.39	−1.89
Ras·RasGAP	+1.04	−0.82	−0.96	−0.88	−0.27	−1.89
	P_α	$O_{1\alpha}$	$O_{2\alpha}$	O'_5		$\sum_\alpha$
Ras	+1.35	−0.77	−0.80	−0.68		−0.90
Ras·RasGAP	+1.24	−0.72	−0.77	−0.73		−0.98
	C'_5	H'_5	H'_5	C'_4		$\sum_{methyl}$
Ras	+0.10	+0.05	+0.09	−0.01		+0.23
Ras·RasGAP	+0.09	+0.05	+0.07	+0.01		+0.22

The atom names are defined in Fig. 2. All partial charges are given in the unit of the elementary charge e_0. The rows correspond to γ-, β-, α-phosphate and the methyl group. The last column gives the total charge of every group. The mean fluctuation is 0.04 e_0.

Table 3 shows an enhanced shift from γ- to β-phosphate of 0.25 e_0 in the Ras·RasGAP complex in comparison to Ras

Table 3
The total charges of γ-, β-, α-phosphate and the methyl group are given in the unit of the elementary charge

	P_γ		P_β		P_α		Methyl
GTP solvent	−1.60	0.16 →	−1.48	0.25 ←	−1.02	0.13 ←	+0.10
Ras	−1.44	0.25 →	−1.89	0.16 ←	−0.90	0.12 ←	+0.23
Ras·RasGAP	−1.35		−1.89		−0.98		+0.22

The direction of the electron shifts is indicated by the arrows. The magnitude of the shifts is shown by the values above the arrows. The mean fluctuation is 0.04 e_0.

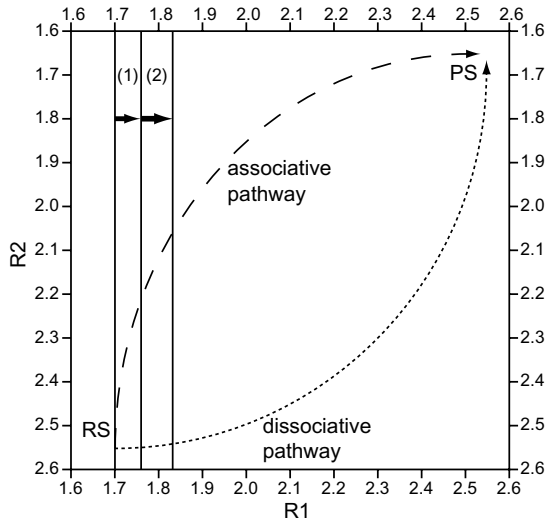

Fig. 4. Computed influence of Ras and Ras·RasGAP on the reaction pathway. By defining a reaction coordinate R1 as the distance between P_γ and $O_{3\beta}$ and R2 as the distance between P_γ and the nucleophilically attacking water molecule (see [14]), we see that Ras (1) is moving the reaction coordinate R1 of the reactant state (RS) towards the product state (PS). The change of R2 was not considered. In the Ras·RasGAP complex (2), R1 is even more forced towards the PS. In both cases, the ground state of the complexes comes closer to a transition state.

without GAP (0.16 e_0). In contrast, more electrons are shifted from α- to β-phosphate when GAP is absent (0.25 e_0 in Ras and 0.16 e_0 in Ras·RasGAP). The observed electron shift from γ- to β-phosphate is a precondition for weakening the bond between P_γ and $O_{3\beta}$. In both complexes the charges' distributions of α-β-phosphate are already close to the charge distribution of the product state.

The enzyme-substrate complex Ras·GTP forces the reactant state of TP towards a transition state. The interaction with GAP consolidates the effect [14]. This is illustrated in Fig. 4 by considering two reaction coordinates, R1 as the distance between P_γ and $O_{3\beta}$ and R2 as the distance between P_γ and the nucleophilically attacking water molecule. Ras and even more Ras·RasGAP drive the ground state of TP closer to a transition state. The change of the charge distribution supports this observation. Our simulations have not reached any transition state as the setup does not aim to reproduce the complete reaction pathway of hydrolysis.

Primarily, the observed changes have to be attributed to the modification of the electrostatic field by forming a complex with GAP. We analysed in detail the influence of surrounding atoms onto the electric field inside the quantum box, especially the role of the positively charged arginine finger. We calculated the electric field vectors at the positions of the QM atoms induced by all surrounding MM atoms of the protein and solvent. The intramolecular interaction of the QM atoms was omitted in order to obtain the influence of the environment on the substrate. The electrostatic field vectors at the position of the nuclei were calculated for each energy-minimised QM/MM structure and averaged over all snapshots. For compari-

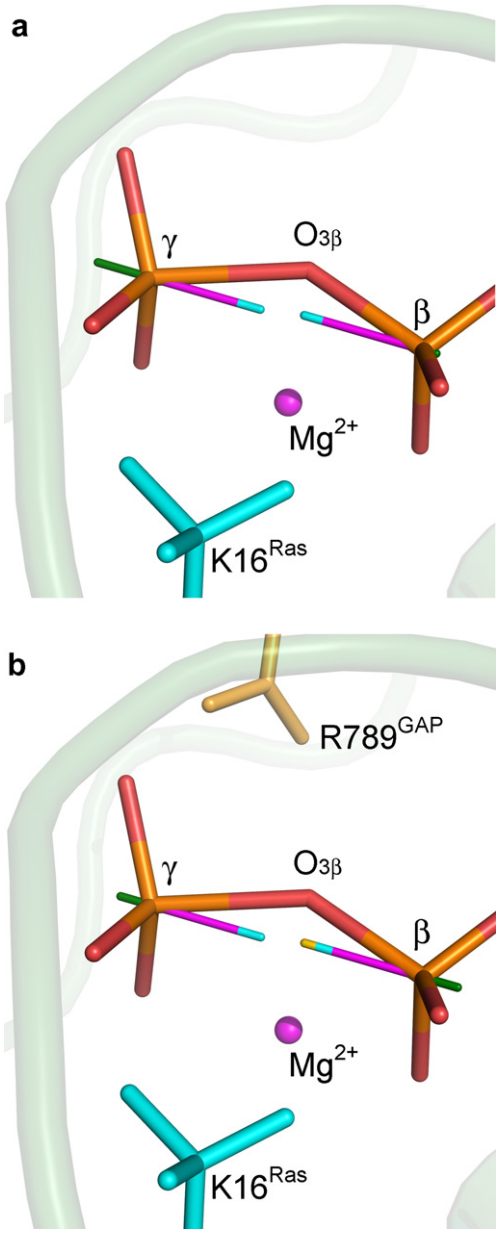

Fig. 5. Sample-averaged electrostatic forces from the MM environment onto electrons in the γ-and β-phosphate of TP in Ras (a) and RasGAP (b). The vectors were projected onto the connecting line between the phosphates and equally scaled for both cases. The contribution of $K16^{Ras}$ is shown in cyan, of Mg^{2+} in magenta, of $R789^{GAP}$ in orange and of all other protein and solvent atoms in green. The influence of $R789^{GAP}$ is negligible. The contributions of Mg^{2+} and $K16^{Ras}$ are identical in Ras and RasGAP, only the solvent contribution is different. Hence, the increment in the driving force for the electron shift from γ to β is solely due to elimination of water from the binding niche by GAP.

son with electron shifts, the field vectors **E** were averaged over the atoms of the respective phosphate group, the force on electrons is calculated as $\mathbf{F} = -\mathbf{E} \cdot e_0$, and projected onto the connecting lines between γ- and β-phosphorus atoms. The projections discussed below are in the nano Newton range with errors <1 nN. We can separate all components forming the electric field. The contributions of the magnesium ion, $K16^{Ras}$, $R789^{GAP}$ and the protein-water-environment to the full force vector are shown in Fig. 5. As the electric forces at α-phosphate are negligible, the focus is placed on β- and γ-phosphate.

The electrostatic force on electrons of γ-phosphate tends to shift them towards β-phosphate in Ras and Ras·RasGAP and originates mainly from Mg^{2+} and to a lesser extent from $K16^{Ras}$. The forces from Mg^{2+} (4 nN) and $K16^{Ras}$ (1 nN) are identical in Ras and Ras·RasGAP. The two ions also exert a somewhat smaller electrostatic force in the opposite direction from β-towards γ-phosphate as they are located between the phosphates. According to Klähn [14], the net shift from γ- to β-phosphate in Ras is essentially due to the excess charge on γ. Note that at either phosphate a small opposite force occurs which derives from other partial charges.

In the Ras·RasGAP complex, the contribution of $R789^{GAP}$ which intrudes the binding niche is negligible at the γ-phosphate and small (−0.5 nN) at the β-phosphate. The crucial difference to Ras is the elimination of water dipoles from the binding niche. Whereas four to six water molecules are in direct contact to γ- and β-phosphate in Ras, only one is found in the Ras·RasGAP complex. Three conserved structural water molecules near the magnesium ion and the α-phosphate are found in both complexes (see Fig. 2).

The waters in Ras exert a force of −1.0 nN at every phosphate group. Based on the above argument, these forces hinder the functional charge shift and hold the electrons on the γ-phosphate in place, see Fig. 5 top. Thus, water weakens the effect of the charges present in the binding niche.

In Ras·RasGAP, however, the electrostatic forces are not obscured by water. Fig. 5 bottom shows a stronger net force (4 nN instead of 3 nN) at the γ-phosphate which explains the larger shift of electron charge away from γ-and towards β-phosphate. At the β-phosphate, the missing water influence reveals a small force from the protein environment that holds electrons in place there and augments the shift. Here, the total force is −3.3 nN instead of −3.9 nN.

4. Discussion

For hydrolysis of GTP to occur, two separate processes must take place: the P_γ–$O_{3\beta}$ bond must be cleaved and a water molecule must bind to P_γ via nucleophilic attack. Model calculations [14] indicate almost equal barriers for both processes in solvent. This implies that either step is optimised on the way from solvent via Ras to Ras·RasGAP conditions where hydrolysis occurs at the highest rate. Here, we have confined ourselves to the reactant state of the cleavage step. Other groups analysed the complete GTP hydrolysis pathway using approximate methods [14] or considering a protein substrate fragment [19] instead of the whole Ras·GTP·RasGAP complex in solvent investigated here. In view of optimal evaluation of the Coulomb interaction, we used the FAMUSAMM algorithm [26–28], which eliminates cut-off artefacts.

For the comprehension of the cleavage step, we performed QM/MM calculations on GTP in Ras and Ras·RasGAP with solvent and first calculated IR spectra of TP. The measured IR data are very sensitive to structural and charge details. Therefore, they provide an ideal check for the quality of computations. We verify our calculated data with the experimental data [5–9]. The TP was treated quantum mechanically. The evaluations focussed on its changes in structure and charge distribution when going from Ras to Ras·RasGAP. The half-open binding niche of Ras·GTP is not deformed by docking GAP and imposes no particular steric conditions on the substrate. Therefore, electrostatic forces are the main cause for the observed changes and the improved catalysis.

The most conspicuous implication is the further decrease of charge on the γ-phosphate by 0.9 e_0 when going from Ras to Ras·RasGAP, at constant charge on the β-phosphate. This

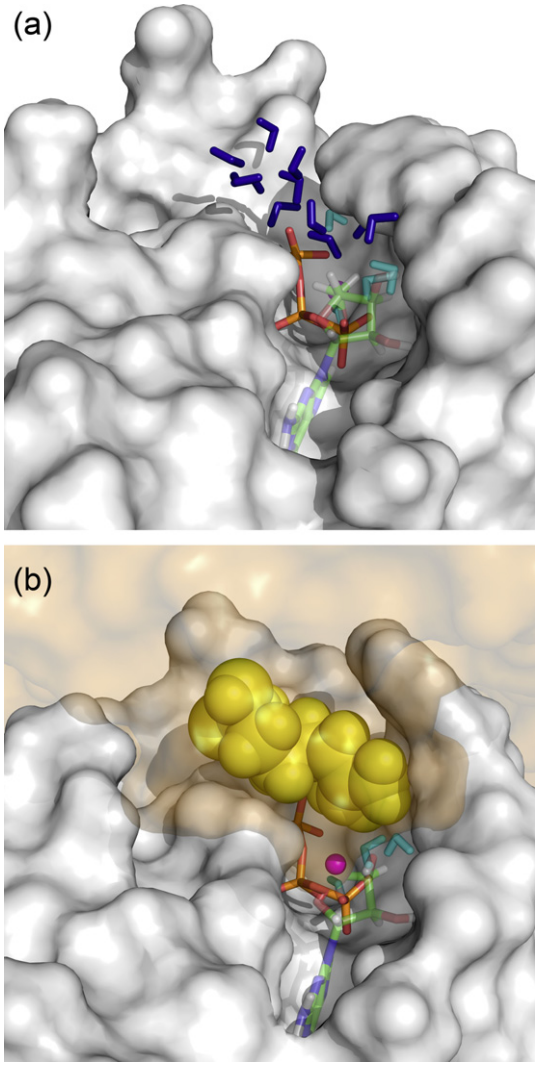

Fig. 6. In the binding niche of Ras (top) the triphosphate is covered by solvent from one side below $P34^{Ras}$ and $Y32^{Ras}$. The water molecules displaced by GAP, especially by $R789^{GAP}$, are shown in dark blue. The *remaining four* water molecules (two waters coordinated at Mg^{2+}, one water at α-phosphate and the nucleophilically attacking water) are shown in cyan. In the Ras·RasGAP complex (bottom) the arginine finger (shown in yellow spheres) eliminates all but one water molecule from γ- and β-phosphate. RasGAP (in orange) covers the binding niche.

completely corresponds to the findings of Grigorenko et al. [17] despite the different theoretical approach and is similar to those of Klähn et al. [20]. It indicates a further approach of the charge distributions to those of transition and product state which are known approximately [14]. As a consequence, we find that the P_γ–$O_{3\beta}$ bond to be cleaved later and the P_γ–P_β distance are already stretched by about 0.1 Å. Fig. 4 demonstrates the approach to the product state without anticipating a particular sequence of events (dissociative vs. associative). Obviously, the structural changes are accompanied by an increase in free energy of GTP as it is transferred to a less probable geometry. This was previously shown by comparison of the eclipse angle of P_γ–P_β in solvent and Ras [20]. In Ras·RasGAP, we find a nearly perfectly eclipsed conformation is part of a non-specified high-energy state. This is explained by the enhanced electrostatic interaction of magnesium with phosphate oxygens.

In the transition state of Ras·RasGAP, the arginine finger points into the binding niche and therefore is proposed to be responsible for the enhanced catalysis ($\approx 10^5$) [4]. It was suggested frequently that it acts via the arginine charge pointing to the TP to be cleaved [8]. Furthermore, it orients $Q61^{Ras}$ and positions the attacking water molecule [38]. Substitution by alanine or lysine greatly reduces the rate enhancement by a factor of 5000 [41]. Only the arginine finger perfectly fits into the binding pocket.

The main result of our investigation is the negligible contribution of the $R789^{GAP}$ positive charge to the electric field at the phosphate positions. The charge helps to anchor arginine in the niche. The catalytic effect, however, is due to displacement of solvent.

In Ras, the binding niche is half-open, $P34^{Ras}$ and $Y32^{Ras}$ being too far away to serve as a tight lid, see Fig. 6 top. Four to six water molecules are in contact with γ and β-phosphate, thus making up 84% of the electrostatic solvent field, the 13–14 waters of the second shell contribute 16%. The waters bear a mean orientation due to the ionic charges, their field is a reaction field which of course weakens the ion field in the niche and can lower the reaction rates [42]. Only in Ras·RasGAP are the unperturbed full electrostatic forces exerted by Mg^{2+} and $K16^{Ras}$ able to catalyse the cleavage step of hydrolysis.

5. Conclusion

The large acceleration of GTP hydrolysis in Ras by docking the activator protein GAP implies optimisation of two steps, cleavage and nucleophilic attack. GAP introduces a charged arginine finger into the binding niche. Our comparative simulation study of the reactant state of GTP in Ras and Ras·RasGAP reveals clear effects altering the substrate towards the transition and product state. At the cleavage step, GAP acts not by the charge of its arginine finger, but by eliminating all solvent molecules but one from the active site. Only as a complex do Ras and GAP form the perfect binding pocket for GTP with optimal electrostatic forces.

Acknowledgements: The authors would like to thank the Deutsche Forschungsgemeinschaft (Project SCHL 127/7) and SFB642 for financial support and the NIC Jülich for providing computing time. They are grateful to C. Kötting for many helpful discussions. All molecular images were produced with PyMOL [43].

References

[1] Barbacid, M. (1987) Ras genes. Annu. Rev. Biochem. 56, 779–827.
[2] Feuerstein, J., Goody, R.S. and Webb, M.R. (1989) The mechanism of guanosine nucleotide hydrolysis by p21 c-Ha-ras. The stereochemical course of the GTPase reaction. J. Biol. Chem. 264 (11), 6188–6190.
[3] Wiesmüller, L. and Wittinghofer, A. (1994) Signal transduction pathways involving Ras. Mini review. Cell Signal. 6, 247–267.
[4] Wittinghofer, A., Scheffzek, K. and Ahmadian, M.R. (1997) The interaction of Ras with GTPase-activating proteins. FEBS Lett. 410 (1), 63–67.
[5] Cepus, V., Scheidig, A., Goody, R. and Gerwert, K. (1998) Time-resolved FTIR studies of the GTPase reaction of H-ras p21 reveal a key role for the beta-phosphate. Biochemistry 37, 10263–10271.
[6] Du, X., Frei, H. and Kim, S.H. (2000) The mechanism of GTP hydrolysis by Ras probed by Fourier transform infrared spectroscopy. J. Biol. Chem. 275 (12), 8492–8500.
[7] Allin, C. and Gerwert, K. (2001) Ras catalyzes GTP hydrolysis by shifting negative charges from gamma- to beta-phosphate as revealed by time-resolved FTIR difference spectroscopy. Biochemistry 40 (10), 3037–3046.
[8] Allin, C., Ahmadian, M.R., Wittinghofer, A. and Gerwert, K. (2001) Monitoring the GAP catalyzed H-Ras GTPase reaction at atomic resolution in real time. Proc. Natl. Acad. Sci. USA 98, 7754–7759.
[9] Kötting, C., Blessenohl, M., Suveyzdis, Y., Goody, R.S., Wittinghofer, A. and Gerwert, K. (2006) A phosphoryl transfer intermediate in the GTPase reaction of Ras in complex with its GTPase-activating protein. Proc. Natl. Acad. Sci. USA 103 (38), 13911–13916.
[10] Kötting, C., Kallenbach, A., Suveyzdis, Y., Wittinghofer, A. and Gerwert, K. (in preparation).
[11] Du, X., Black, G.E., Lecchi, P., Abramson, F.P. and Sprang, S.R. (2004) Kinetic isotope effects in Ras-catalyzed GTP hydrolysis: evidence for a loose transition state. Proc. Natl. Acad. Sci. USA 101 (24), 8858–8863.
[12] Chakrabarti, P.P., Suveyzdis, Y., Wittinghofer, A. and Gerwert, K. (2004) Fourier transform infrared spectroscopy on the Rap-RapGAP reaction, GTPase activation without an arginine finger. J. Biol. Chem. 279 (44), 46226–46233.
[13] Warshel, A. and Parson, W.W. (2001) Dynamics of biochemical and biophysical reactions: insight from computer simulations. Quart. Rev. Bio-phys. 34 (4), 563–679.
[14] Klähn, M., Rosta, E. and Warshel, A. (2006) On the mechanism of hydrolysis of phosphate monoesters dianions in solutions and proteins. J. Am. Chem. Soc. 128 (47), 15310–15323.
[15] Kötting, C. and Gerwert, K. (2004) Time-resolved FTIR studies provide activation free energy, activation enthalpy and activation entropy for GTPase reactions. J. Chem. Phys. 307, 227–232.
[16] Grigorenko, B.L., Rogov, A.V. and Nemukhin, A.V. (2006) Mechanism of triphosphate hydrolysis in aqueous solution: QM/MM simulations in water clusters. J. Phys. Chem. B 110 (9), 4407–4412.
[17] Grigorenko, B.L., Nemukhin, A.V., Shadrina, M.S., Topol, I.A. and Burt, S.K. (2007) Mechanisms of guanosine triphosphate hydrolysis by Ras and Ras-GAP proteins as rationalized by ab initio QM/MM simulations. Proteins 66 (2), 456–466.
[18] Topol, I., Cachau, R., Nemukhin, A., Grigorenko, B. and Burt, S. (2004) Quantum chemical modeling of the GTP hydrolysis by the RAS-GAP protein complex. Biochim. Biophys. Acta, Proteins Proteomics 1700, 125–136.
[19] Grigorenko, B.L., Nemukhin, A.V., Topol, I.A., Cachau, R.E. and Burt, S.K. (2005) QM/MM modeling the Ras-GAP catalyzed hydrolysis of guanosine triphosphate. Proteins 60 (3), 495–503.
[20] Klähn, M., Schlitter, J. and Gerwert, K. (2005) Theoretical IR Spectroscopy Based on QM/MM Calculations Provides Changes in Charge Distribution, Bond Lengths, and Bond Angles of the GTP Ligand Induced by the Ras-Protein. Biophys. J. 88, 3829–3844.
[21] Futatsugi, N., Hata, M., Hoshino, T. and Tsuda, M. (1999) Ab initio study of the role of lysine 16 for the molecular switching mechanism of Ras protein p21. Biophys. J. 77, 3287–3292.

[22] Futatsugi, N. and Tsuda, M. (2001) Molecular dynamics simulations of Gly-12 → Val mutant of p21(ras): dynamic inhibition mechanism. Biophys. J. 81 (6), 3483–3488.
[23] Katagiri, D., Hata, M., Itoh, T., Neya, S. and Hoshino, T. (2003) Atomic-scale mechanism of the GTP → GDP hydrolysis reaction by the Gi alpha 1 protein. J. Phys. Chem. B 107, 3278–3283.
[24] Eichinger, M., Heller, H., Grubmüller, H. (2000). EGO – an efficient molecular dynamics program and its application to protein dynamics simulations. In Esser, R., Grassberger, P., Grotendorst, J. (Eds.). Workshop on Molecular Dynamics on Parallel Computers (pp. 154–174). Singapore: World Scientific.
[25] CPMD, Copyright IBM Corp 1990–2006, Copyright MPI für Festkörper-forschung Stuttgart 1997–2001.
[26] Mathias, G., Egwolf, B., Nonella, M. and Tavan, P. (2003) A fast multi-pole method combined with a reaction field for long-range electrostatics in molecular dynamics simulations: the effects of truncation on the properties of water. J. Chem. Phys. 118, 10847–10860.
[27] Niedermeier, C. and Tavan, P. (1994) A structure adapted multipole method for electrostatic interactions in protein dynamics. J. Chem. Phys. 101, 734–748.
[28] Niedermeier, C. and Tavan, P. (1996) Fast version of the structure adapted multipole method-efficient calculation of electrostatic forces in protein dynamics. Mol. Simulat. 17, 57–66.
[29] Eichinger, M., Tavan, P., Hutter, J. and Parrinello, M. (1999) A hybrid method for solutes in complex solvents: density functional theory combined with empirical force fields. J. Chem. Phys. 110, 10452–10467.
[30] Singh, U. and Kollman, P. (1984) An approach to computing electrostatic charges for molecules. J. Comput. Chem. 5 (2), 129–145.
[31] Becke, A. (1988) Density-functional exchange-energy approximation with correct asymptotic behavior. Phys. Rev. A 38, 3098–3100.
[32] Perdew, J. (1986) Density-functional approximation for the correlation energy of the inhomogeneous electron gas. Phys. Rev. B: Condens. Mat. Mater. Phys. 33 (12), 8822–8824.
[33] Hartwigsen, C., Goedecker, S. and Hutter, J. (1998) Relativistic separable dual-space Gaussian Pseudopotentials from H to Rn. Phys. Rev. B: Condens. Mat. Mater. Phys. 58, 3641–3662.
[34] Mackerell, A., Bashford, D., Bellott, M., Dunbrack, R., Evanseck, J., Field, M., Fischer, S., Gao, J., Guo, H., Ha, S., Joseph-McCarthy, D., Kuchnir, L., Kuczera, K., Lau, F., Mattos, C., Michnick, S., Ngo, T., Nguyen, D., Prodhom, B., Reiher, W., Roux, B., Schlenkrich, M., Smith, J., Stote, R. and Straub, J. (1998) All-atom empirical potential for molecular modeling and dynamics studies of proteins. J. Phys. Chem. B 102, 3586–3616.
[35] Nonella, M., Mathias, G. and Tavan, P. (2003) Infrared spectrum of *p*-benzoquinone in water obtained from a QM/MM hybrid molecular dynamics simulation. J. Phys. Chem. A 107, 8638–8647.
[36] Klähn, M., Mathias, G., Kötting, C., Nonella, M., Schlitter, J., Gerwert, K. and Tavan, P. (2004) IR spectra of phosphate ions in aqueous solution: predictions of a DFT/MM approach compared with observations. J. Phys. Chem. A 108, 6186–6194.
[37] Scheidig, A., Burmester, C. and Goody, R. (1999) The pre-hydrolysis state of p21(ras) in complex with GTP: new insights into the role of water molecules in the GTP hydrolysis reaction of ras-like proteins. Structure 7, 1311–1324.
[38] Scheffzek, K., Ahmadian, M., Kabsch, W., Wiesmüller, L., Lautwein, A., Schmitz, F. and Wittinghofer, A. (1997) The Ras · RasGap complex – structural basis for GTPase activation and its loss in oncogenic Ras mutants. Science 277, 333–338.
[39] Vriend, G. (1990) WHAT IF: a molecular modeling and drug design program. J. Mol. Graphics Modell. 8 (1), 52–56, 29.
[40] Cavalli, A. and Carloni, P. (2002) Enzymatic GTP hydrolysis: insights from an ab initio molecular dynamics study. J. Am. Chem. Soc. 124, 3763–3768.
[41] Ahmadian, M.R., Stege, P., Scheffzek, K. and Wittinghofer, A. (1997) Confirmation of the arginine-finger hypothesis for the GAP-stimulated GTP-hydrolysis reaction of Ras. Nat. Struct. Biol. 4 (9), 686–689.
[42] Fersht, A. (2004) Structure and Mechanism in Protein Science. Guide to Enzyme Catalysis and Protein Folding, W.H. Freeman & Co. Ltd..
[43] DeLano, W.L. (2002) The PyMOL Molecular Graphics System, DeLano Scientific, Palo Alto, CA, USA.